· Article · Advances in Polar Science
doi: 10.12429/j.advps.2024.0003 December 2024 Vol. 35 No. 4: 438-448

The enhanced synoptic variation in sea ice over Pacific sector of Arctic Ocean during summer half year

LI Yijiao[1], JIANG Zhina[1,2*], DAI Guokun[2] & DING Minghu[1]

[1] State Key Laboratory of Severe Weather and Institute of Global Change and Polar Meteorology, Chinese Academy of Meteorological Sciences, Beijing 100081, China;
[2] Key Laboratory of Polar Atmosphere-ocean-ice System for Weather and Climate, Ministry of Education, Department of Atmospheric and Oceanic Sciences and Institute of Atmospheric Sciences, Fudan University, Shanghai 200438, China

Received 30 January 2024; accepted 21 May 2024; published online 30 December 2024

Abstract This study investigates the synoptic Arctic sea ice variation during the summer half year based on a regional daily sea ice concentration (SIC) tendency index during 1979–2021. Results indicate an enhancement in synoptic SIC variation over the Pacific sector of Arctic Ocean, with the maximum amplitude concentrating along the sea ice edge to covering a larger domain. Most synoptic severe sea ice variations occur for a single day or 2–3 d, typically starting after mid-June and ending in mid-November over Beaufort–Chukchi seas. However, there is a clear shift in ending time over the East Siberian–Laptev seas from early October to early November. Further analysis suggests that wind-driven sea ice drift may significantly contribute to the amplification of synoptic sea ice variation. This result contributes to our understanding of regional Arctic sea ice predictability, particularly in relation to the Arctic northeast shipping passage.

Keywords **sea ice**, **synoptic variability**, **Arctic**, **enhancement**, **summer**

Citation: Li Y J, Jiang Z N, Dai G K, et al. The enhanced synoptic variation in sea ice over Pacific sector of Arctic Ocean during summer half year. Adv Polar Sci, 2024, 35(4): 438-448, doi: 10.12429/j.advps.2024.0003

1 Introduction

Arctic sea ice, as an important part of earth system, has profound impacts on human activities and ecosystems in the Arctic and midlatitude (Bhatt et al., 2010; Chen and Sun, 2024; Chen et al., 2021; Liu et al., 2017; Post et al., 2013; Wu and Li, 2021; Zhang et al., 2022). It is noteworthy that Arctic sea ice is declining and thinning during the period of satellite observations, whose decline has been accelerating since around 2000 (Comiso et al., 2008; Lee et al., 2017; Serreze and Stroeve, 2015; Serreze et al., 2007; Stroeve et al., 2007), with the most extreme decline seen in September (Simmonds, 2015). The Arctic is expected to become essentially ice-free during summer by about midcentury (Holland et al., 2006; Notz and Stroeve, 2016), and even earlier (Guarino et al., 2020).

There is a lot of literature that examines sea ice loss on the interannual to decadal time scales (Bi et al., 2021; Blackport et al., 2019; Comiso et al., 2017; Francis and Wu, 2020; Kwok, 2018; Liang et al., 2018; Park H S et al., 2015; Parkinson and Cavalieri, 2012; Wang et al., 2023; You et al., 2022), and recently on the intraseasonal time scale (Chen et al., 2018; Gong and Luo, 2017; Jiang et al., 2021; Luo et al., 2017; Mohammadi-Aragh et al., 2018; Qian et al., 2020; Tian et al., 2022; Wang et al., 2020; Yang et al., 2022; Zheng et al., 2022). Younger and thinner sea ice melts faster (Tschudi et al., 2016), which may have played a role in the dramatic reduction in Arctic sea ice in recent September (Stroeve et al., 2008; Yang and Magnusdottir, 2017). Though great progress has been achieved that links sea ice decline on the intraseasonal time scale to large scale

* Corresponding author. ORCID: 0000-0002-7272-8821. E-mail: jiangzn@cma.gov.cn.

atmospheric circulation, in most Arctic regions in the summertime, sea ice forecast skill is lower on extreme sea ice loss days than on nonextreme days (McGraw et al., 2022). Therefore, it is necessary to present a qualitative estimation of synoptic sea ice variation, so as to better understand the predictability of Arctic sea ice on the intraseasonal time scale.

The paper is organized as follows. Section 2 describes the data and methods used in this study. Section 3 shows the general changes of regional sea ice concentration (SIC). The characteristics of synoptic regional SIC variation under different climatic backgrounds are explored in Section 4. Summary and concluding remarks are presented in Section 5.

2 Data and method

2.1 Data

In this study, the daily SIC (> 15%) with a spatial resolution of 25 km from the National Snow and Ice Data Center (NSIDC) is adopted to explore the sea ice variation (Cavalieri et al., 2012). We also use the NSIDC daily 25-km EASE-Grid sea ice motion dataset (Tschudi et al., 2019). In this investigation, we mainly focus on the summer half year, which includes summer (June to August) and autumn (September to November) ranging from 1979 to 2021.

2.2 Method

Anomalies of variables are calculated by subtracting the seasonal cycle at each grid point. In order to see the temporal evolution of Arctic sea ice, the seasonal mean SIC index is constructed by averaging the daily SIC anomalies weighted by cosine (latitude) over the Arctic Ocean poleward of 52°N. A linear downward trend of Arctic SIC in summer and autumn is clearly seen in Figure 1, in which the autumn Arctic sea ice has a larger retreat ($-0.42\%\cdot a^{-1}$) than the summer ($-0.39\%\cdot a^{-1}$). In addition, a significant trend transition can be seen in 2001 (2002) in summer (autumn), which is verified by the Mann-Kendall test (Kendall, 1975; Mann, 1945). Considering that there is a significant Arctic sea ice trend transition before and after the early 2000s, we divide the satellite record from 1979 to 2021 into two periods before and after the turning point, labeled as P1 and P2, respectively. In summer, Arctic sea ice has a larger retreat of $-0.40\%\cdot a^{-1}$ during P2 (2002–2021) than that of $-0.28\%\cdot a^{-1}$ during P1 (1979–2001). As well, in autumn, Arctic sea ice has a larger retreat of $-0.44\%\cdot a^{-1}$ during P2 (2003–2021) than that of $-0.21\%\cdot a^{-1}$ during P1 (1979–2002).

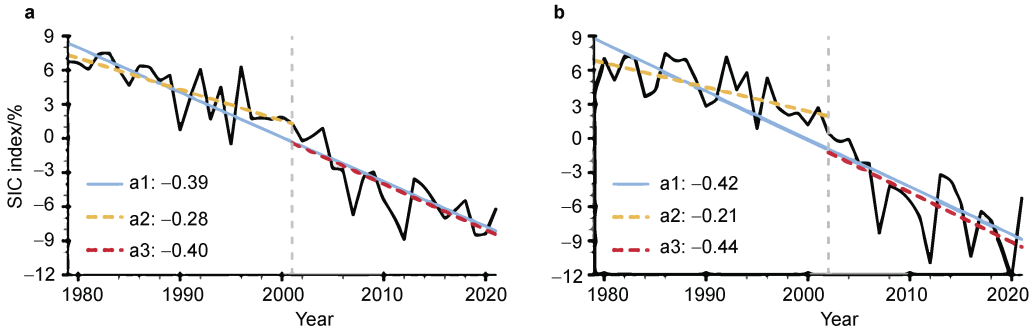

Figure 1 Time series of the Arctic SIC index during 1979–2021 (black line) for summer (**a**) and autumn (**b**), in which the blue line represents the linear trend during 1979–2021, and yellow (red) dashed line represents the linear trend during P1 (P2), respectively.

Because we focus on the synoptic SIC changes, the linear trend during 1979–2021 is also removed for each calendar day in the following calculation. Due to the average e-folding time scale of daily SIC is about a week (Park D S R et al., 2015), the synoptic sea ice variation is evaluated based on a daily SIC tendency index, which is approximated by the forward difference of SIC anomaly along the time dimension (Jiang et al., 2021). Regional daily Arctic sea ice tendency index is obtained by averaging the daily SIC tendency index over the given region. We pay much attention to the days with severe sea ice variation, e.g., daily SIC tendency amplitude larger than 1.5 standard deviation, and daily SIC tendency in the lowest and highest 5%. The statistical significance of our composite calculation is evaluated using two-sided Student's *t* test.

3 General changes of Arctic sea ice

Figure 2 shows the Arctic climatological SIC and drift in summer and autumn during P1 and P2, respectively. It is seen that the Arctic sea ice retreats more poleward in autumn than in summer. The most evident difference in climatological SIC between P1 and P2 appears over Eastern Siberian–Laptev seas (ES–L; 100°E–180°, 68°N–85°N) and Beaufort–Chukchi seas (B–C; 180°–240°E, 68°N–85°N), indicating a strong air-ice interaction there. Over these regions another remarkable difference is reflected in the sea ice motion. There is an evident enhancement of Beaufort Gyre and Transpolar Drift Stream from P1 to P2, consistent with Sumata et al. (2023). Due to the different sea ice motions in ES–L and B–C, sea ice features in ES–L and B–C are investigated individually.

As shown in Figure 3, seasonal cycles of regionally-averaged SIC are apparent over these two regions, with minima in September, and maximum in winter owing to their nearly completely covered by sea ice in those months. The regionally-averaged SIC in P2 during the summer half

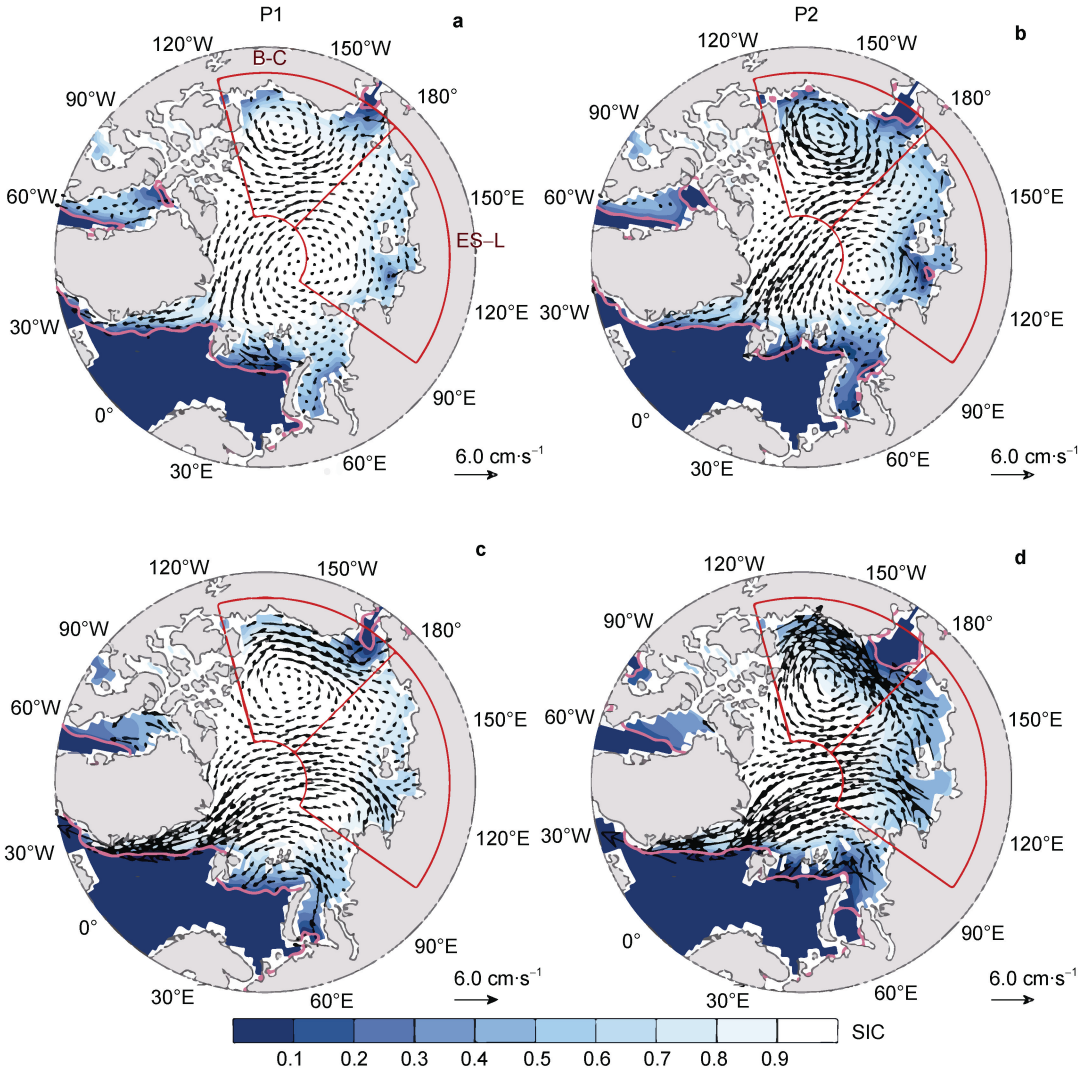

Figure 2 Arctic climatological sea ice concentration (SIC, shaded) and sea ice motion (vector) in summer during P1 (**a**) and P2 (**b**); **c** and **d** are similar to **a** and **b**, respectively, but in autumn. The Eastern Siberian and Laptev seas (ES–L) domain and Beaufort and Chukchi Seas (B–C) domain are framed with red boxes. Pink line represents the sea ice edge (15% in SIC).

year is much smaller than in P1. Consistent with the seasonality of SIC, an evident strong annual SIC variations can be observed in the summer half year. Strong seasonality is also reflected in the SIC trend. The strongest SIC negative trend occurs from September to October, which enhances greatly from P1 to P2. In general, the variation of SIC over ES–L in P2 is the most evident.

Figure 4 shows the spatial distributions of intraseasonal SIC variability during P1 and P2 in summer and autumn, respectively. It is found that the majority of the large SIC intraseasonal variability appears along the sea ice margin, namely northern Barents, Kara, Laptev, East Siberian, Chukchi and Beaufort seas. Compared with P1, the maximum center of SIC intraseasonal variability during P2 moves more poleward. Moreover, the intensity of SIC intraseasonal variability during P2 increases evidently over ES–L and B–C, especially in autumn (Figure 4e).

4 Synoptic sea ice concentration variation

To get a better knowledge about synoptic sea ice variation, Figure 5 shows the distribution of days with different standard deviation intervals of daily SIC tendency over ES–L and B–C, respectively. A common feature is that the days with daily SIC tendency index amplitude larger than one standard deviation increase evidently from P1 to P2. On the contrary, the days with daily SIC tendency index amplitude less than one standard deviation decrease from P1 to P2, which is more evident in autumn (Figures 5c and 5d). To be specific, in autumn over ES–L there are about 1100 d within 0.5 standard deviation in P1, which decreases to about 700 d in P2, with the reduction rate of over 30%.

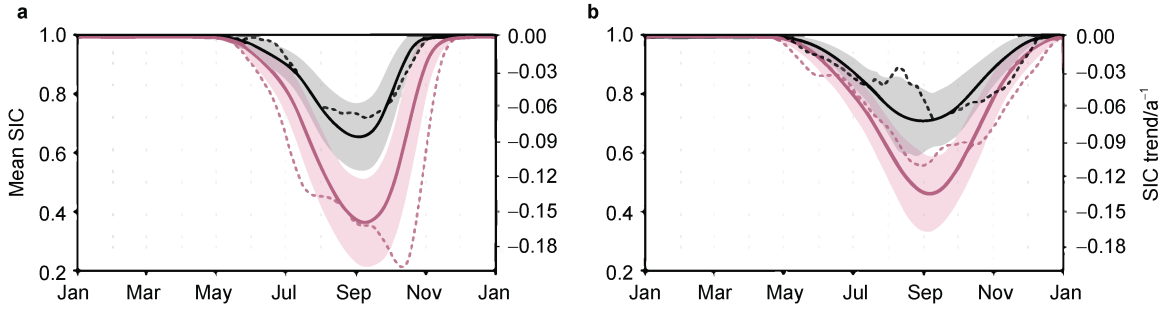

Figure 3 The mean (solid curves) with one standard deviation (shading) and the linear trend (dashed curves; units: a^{-1}) of regionally-averaged SIC as a function of calendar days over Eastern Siberian and Laptev seas (ES–L) (**a**); and Beaufort and Chukchi seas (B–C) (**b**). The left ordinate is for the mean and standard deviation, and the ordinate for the linear trend is shown on the right. Black for P1 and pink for P2.

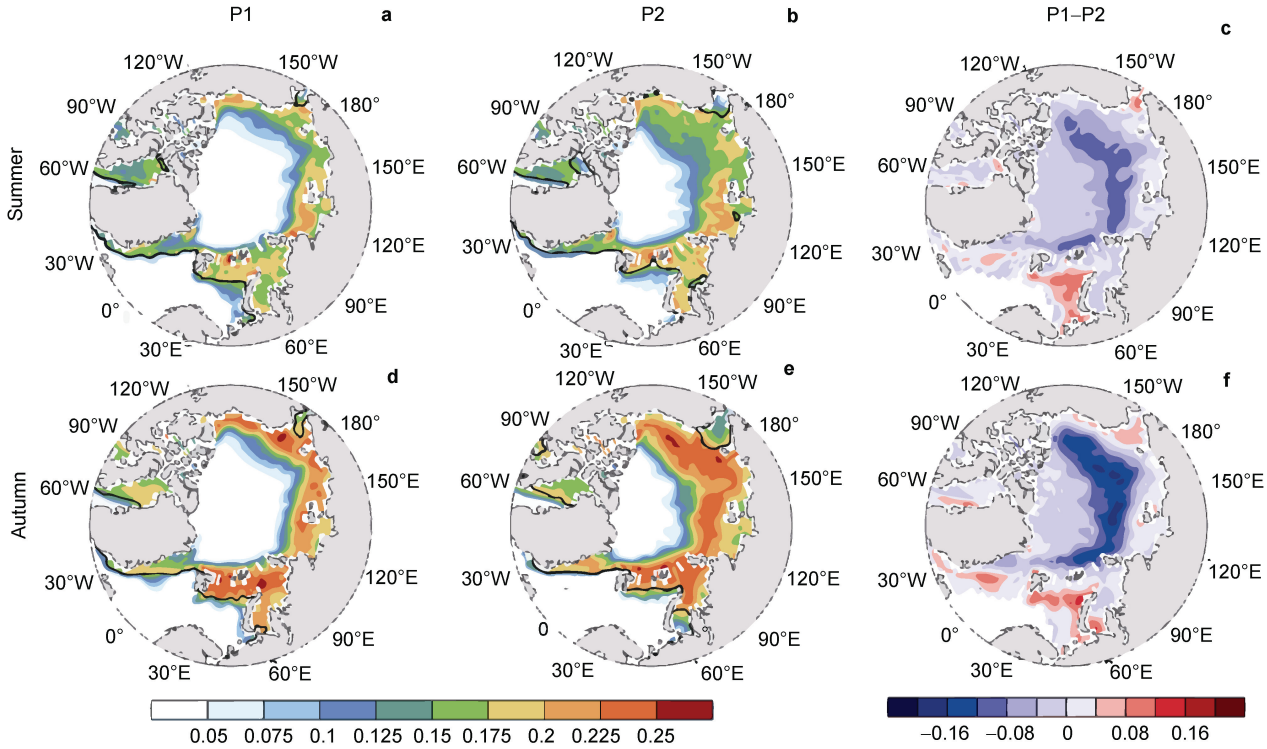

Figure 4 Spatial distribution of Arctic SIC intraseasonal variability in summer during P1 (**a**), P2 (**b**), P1 minus P2 (**c**); **d**, **e**, **f** are similar to **a**, **b**, **c**, but in autumn.

This implies that the synoptic Arctic sea ice variation becomes more intense in a warmer climate.

Moreover, the duration of severe synoptic sea ice variation with amplitude larger than 1.5 standard deviation is illustrated in Figures 6 and 7, respectively. It is seen that for severe sea ice loss event (Figure 6), the most common duration is single-day, and then 2–3 d. Compared with P1, not only the single-day sea ice loss events increase in P2, but the persistent sea ice loss events also increase. In summer, there are about 100 single-day sea ice loss events over ES–L during P1, which increase up to 130 single-day sea ice loss events during P2, with the increasing rate of 30%. The increasing rate of single-day sea ice loss events over B–C reaches nearly 50%. Similarly, the persistent sea ice loss events over these two regions also can increase by 50%. In autumn, the 3-day sea ice loss events over ES–L and the 2-day sea ice loss events over B–C even increase twice. For severe sea ice gain, the increasing rate of single-day events can reach at least 30%. The 2-day and 3-day persistent sea ice gain events in summer over ES–L and B–C also increase by about 20%, as well as in autumn over B–C. In addition, it is noteworthy that more persistent severe sea ice loss and gain events (longer than 5 d) appear over ES–L in autumn, with much more in P2 than in P1 (Figures 6c and 7c).

Figure 8 shows the dates with severe sea ice variation during the summer half year. It is seen that the severe daily SIC variation mostly occurs after mid-June over ES–L,

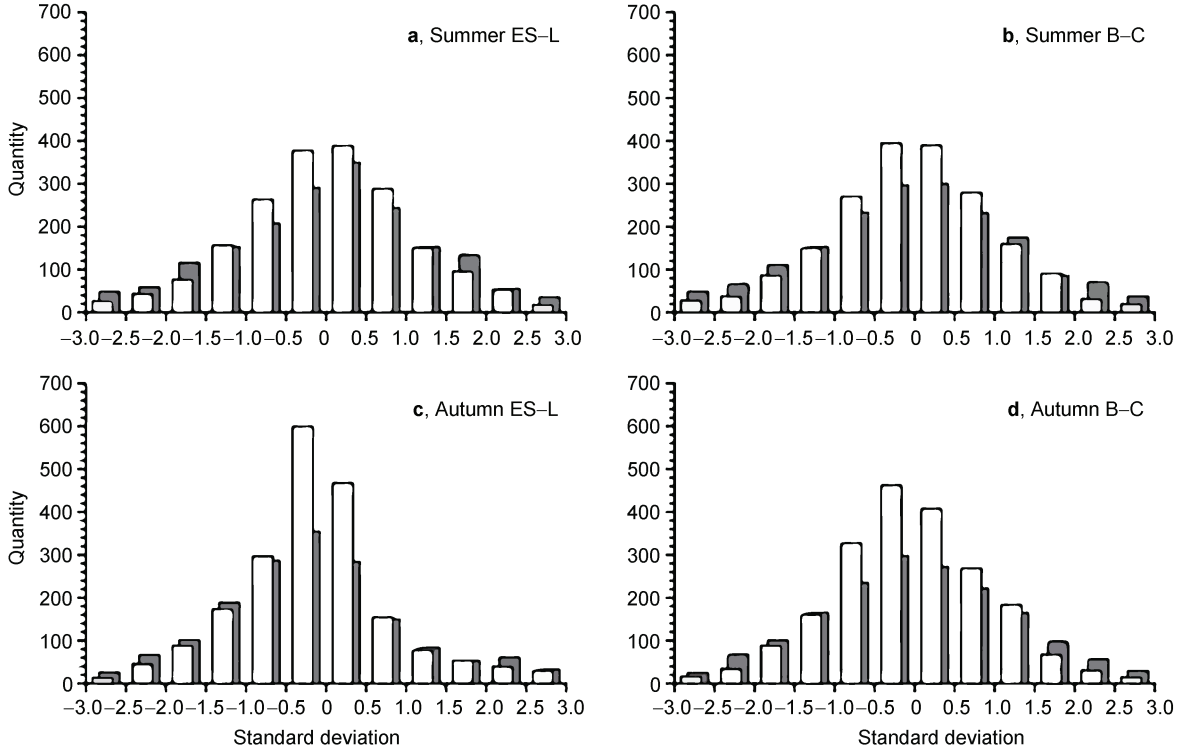

Figure 5 Distribution of days with different standard deviation interval of daily SIC tendency in summer over Eastern Siberian and Laptev seas (ES–L) (**a**); and Beaufort and Chukchi seas (B–C) (**b**); **c** and **d** are similar to **a** and **b**, respectively, but in autumn. Grey bars for P1 and blank bars for P2.

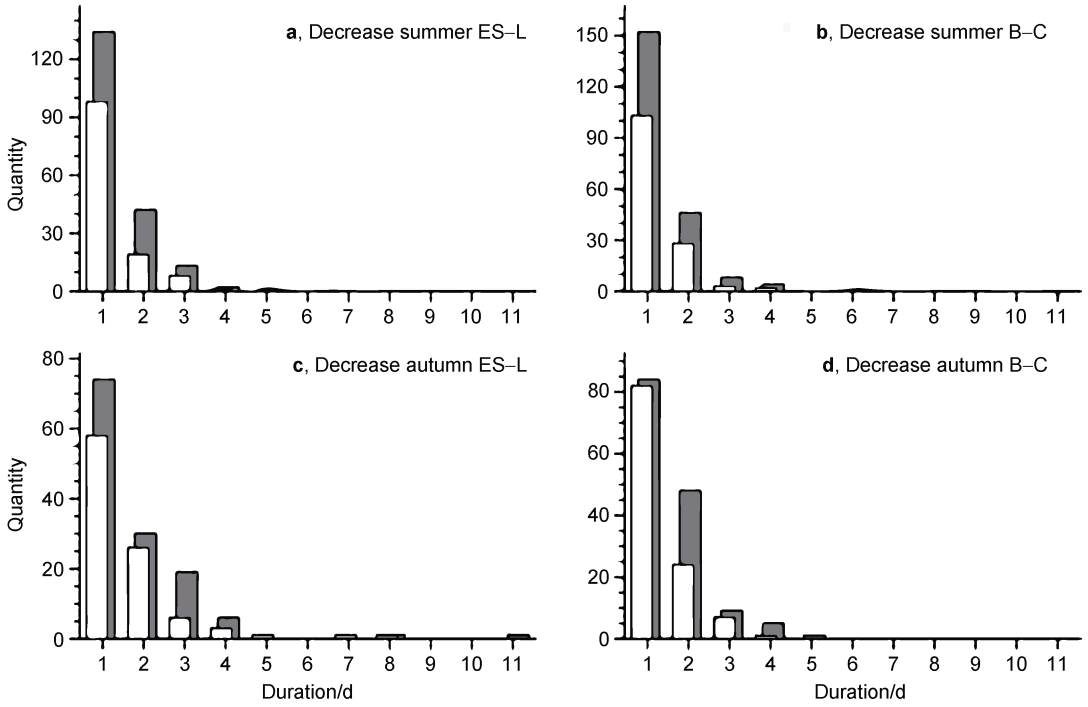

Figure 6 Number of events with different durations of daily SIC tendency less than negative 1.5 standard deviation in summer for Eastern Siberian and Laptev seas (ES–L) (**a**); and Beaufort and Chukchi seas (B–C) (**b**); **c** and **d** are similar to **a** and **b**, respectively, but in autumn. Grey bars for P1 and blank bars for P2. *X*-axis represents duration and *y*-axis is for event number.

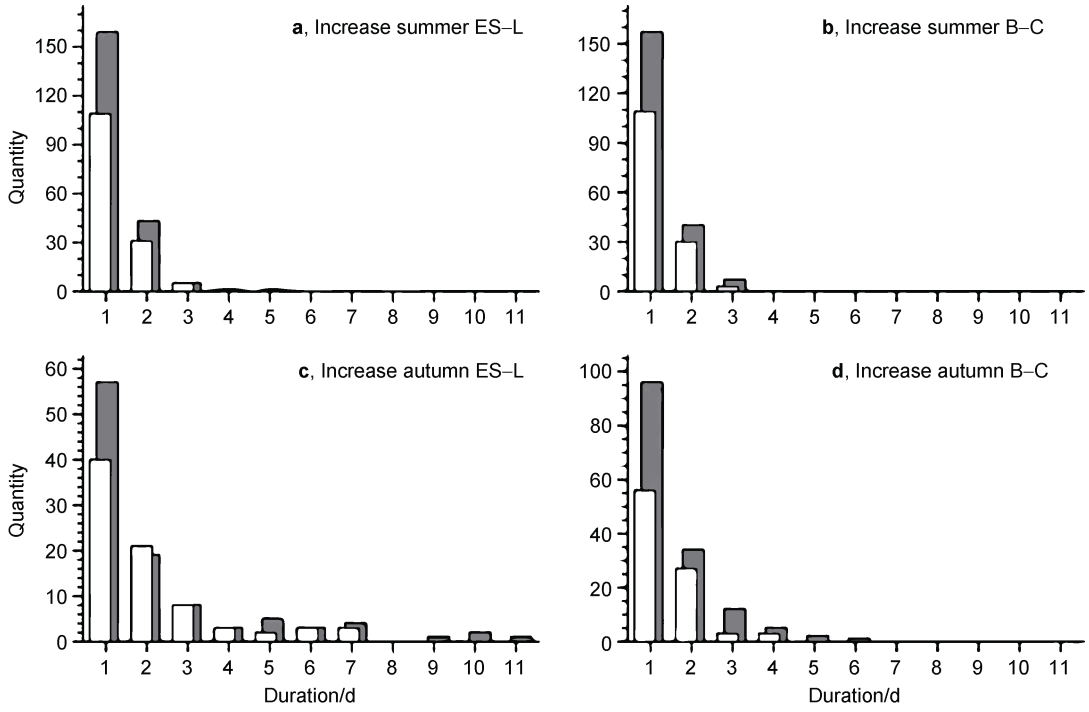

Figure 7 Similar to Figure 6, but of daily SIC tendency larger than 1.5 standard deviation. Grey bars for P1 and blank bars for P2.

which ends before early October during P1 and postpones to early November during P2 (Figures 8a and 8c). However, there is little change about the date of extreme sea ice loss and gain over B–C, which mostly occurs after mid-June and ends in November (Figures 8b and 8d). Another interesting finding is that a large number of days of persistent extreme SIC gain concentrate in October over ES–L (Figure 8c), which possibly contributes to the recovery of sea ice over that region.

To gain insight into the spatial distribution of severe sea ice variation, Figure 9 presents the composite SIC tendency and anomalous sea ice motion for severe sea ice loss/gain days in summer. We can find that during P1 the maximum daily sea ice loss with the amplitude of 6%·d^{-1} mainly occurs along the sea ice border (Figures 9a and 9b), which spreads poleward and dominates a larger domain in P2 (Figures 9e and 9f). The enhanced Transpolar Drift Stream makes contributions to severe sea ice loss, which is in line with Spreen et al. (2011) and Zhang et al. (2021). Similarly, the maximum daily sea ice gain with the amplitude of 5%·d^{-1} also mainly occurs along the sea ice border during P1 (Figures 9c and 9d) and spreads to a larger area during P2 (Figures 9g and 9h). Anomalous sea ice motion is favorable for the sea ice expanding towards the marginal sea, which strengthens during P2.

When we turn to see the extreme sea ice variation in autumn (Figure 10), we find that the maximum daily sea ice loss with the amplitude of 5%·d^{-1} also mainly occurs along the sea ice border (Figures 10a and 10b) in P1, spreading poleward in P2 (Figures 10e and 10f). The maximum amplitude of extreme daily sea ice loss is similar in summer and autumn. However, the maximum amplitude of extreme daily sea ice gain becomes larger with the amplitude of 7%·d^{-1} in autumn than in summer. In addition, sea ice drift for extreme sea ice variation enhances greatly in autumn, which implies dynamic transport may play more important role for synoptic sea ice variation in a warmer climate.

5 Summary and discussion

In this study, we compare the changes of Arctic synoptic sea ice variation during 1979–2021 in the summer half year before and after sea ice trend transition, labelled as P1 and P2, respectively. Results show that synoptic SIC variation enhances greatly in P2 compared with P1. The maximum daily sea ice variation in summer with the amplitude of 5%·d^{-1} mainly occurs along the sea ice border in P1, covering a larger area in P2. In autumn, the maximum daily sea ice variation can reach up to the amplitude of 7%·d^{-1}, which is mainly along the sea ice border in P1, covering a larger area in P2. In addition, both the single-day and persistent sea ice variation events increase in P2, with the increasing rate at least 30% compared with P1. Most synoptic severe sea ice variations start after mid-June and end in mid-November over Beaufort–Chukchi seas. However, there is a clear shift in ending time over the East Siberian–Laptev seas from early October to early November.

The enhancement of synoptic sea ice variation is partly related to the dynamic drift of sea ice motion (Jiang et al., 2021). Furthermore, the synoptic SIC variation may be related to the longwave and shortwave radiation, latent heat

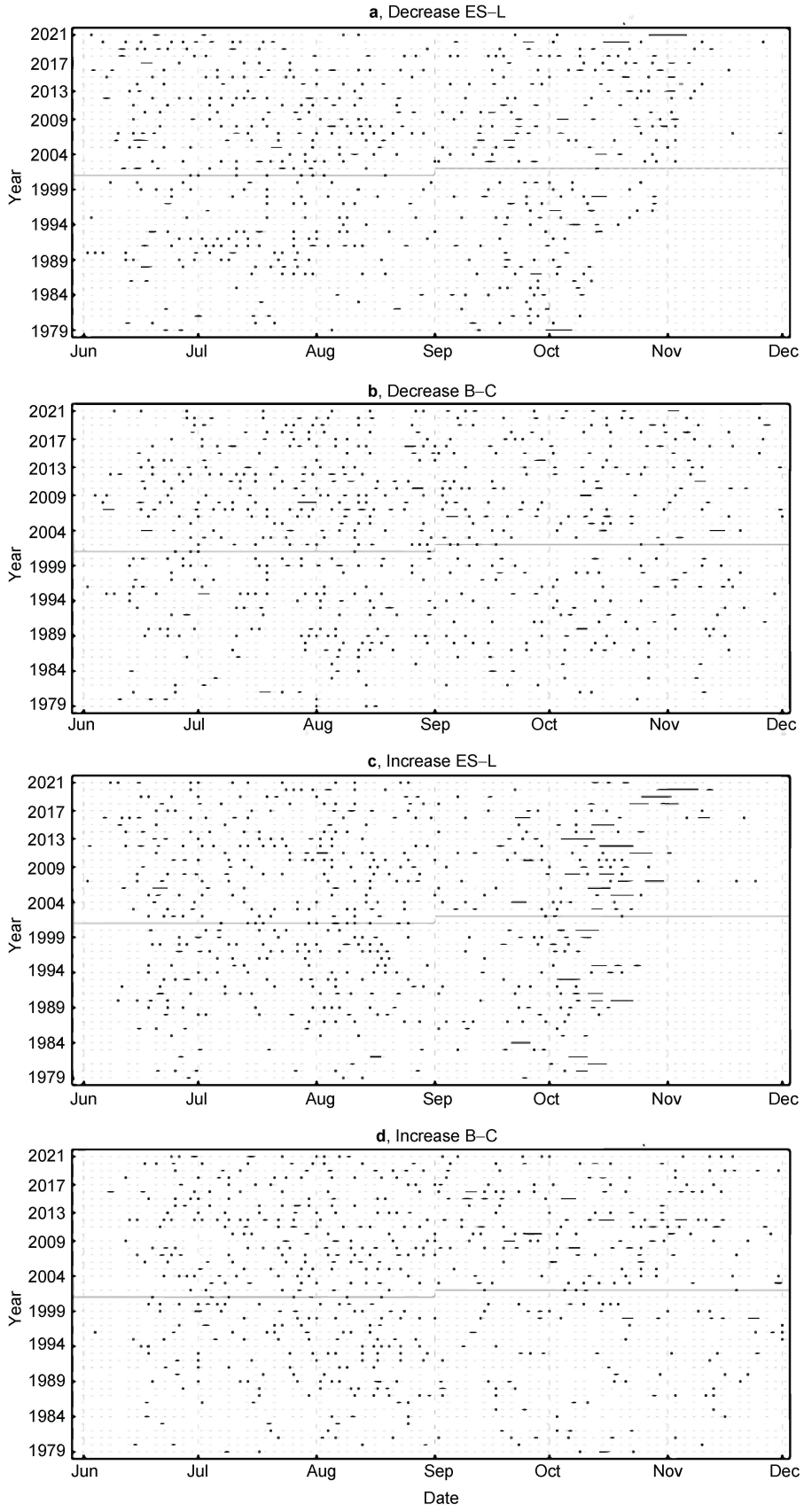

Figure 8 Date with severe sea ice variation for: **a**, extreme sea ice loss over ES–L; **b**, extreme sea ice loss over B–C; **c**, extreme sea ice gain over ES–L; **d**, extreme sea ice gain over B–C. The length represents persistence of days.

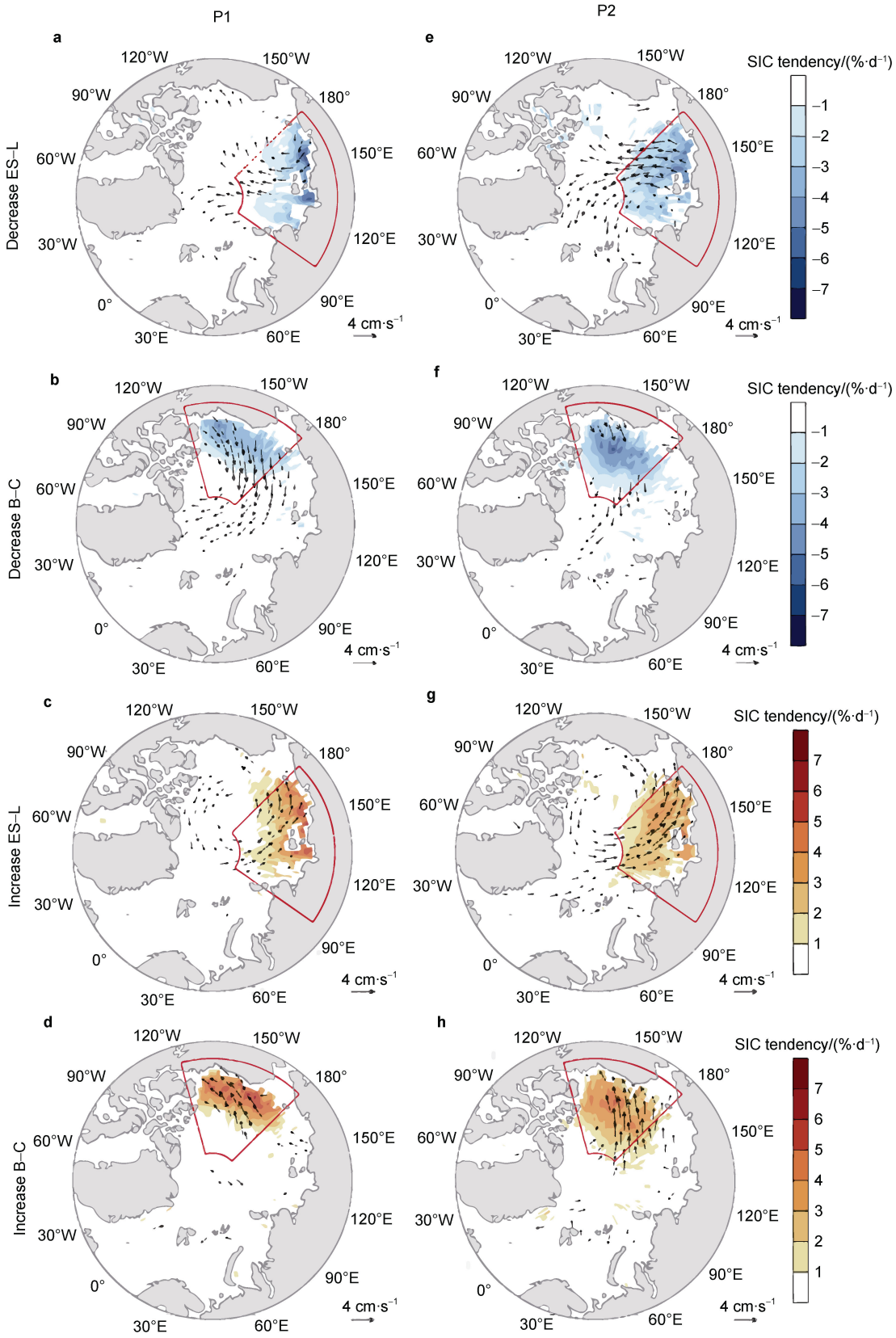

Figure 9 Composites of daily SIC tendency (shaded; unit: %·d^{-1}) and anomalous sea ice motion (vector) in summer for: **a**, sea ice loss over ES–L during P1; **b**, sea ice loss over B–C during P1; **c**, sea ice gain over ES-L during P1; **d**, sea ice gain over B–C during P1; **e**, **f**, **g** and **h** similar to **a**, **b**, **c** and **d** but for during P2. Shading and vector indicate statistical significance at p <0.1 level for the Student's t test.

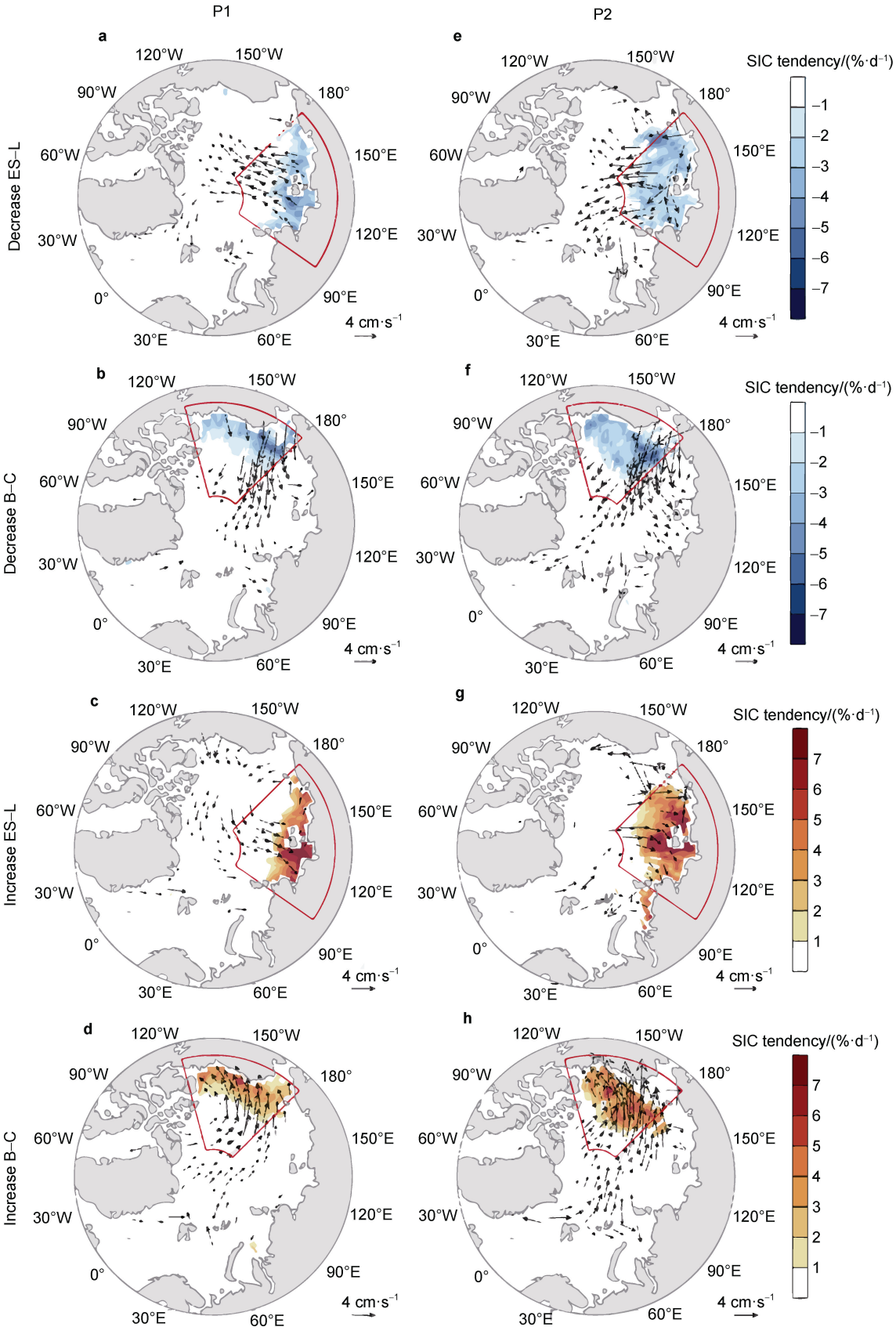

Figure 10 Similar to Figure 9, but in autumn.

flux, sensible heat flux, moisture transport and other processes (Dai et al., 2019, 2023; Jenkins et al., 2024; Jiang et al., 2021; Wang et al., 2020; Zhong et al., 2018). Meanwhile, the synoptic SIC variation may also be associated with the Atlantic multi-decadal oscillation, Pacific decadal oscillation and El Niño-Southern Oscillation (Bi et al., 2021; Luo et al., 2023). Our work implies that accompanied with thinner Arctic sea ice, the interaction between atmosphere and sea ice may become stronger in the following decades. However, this work is just a preliminary exploration to the synoptic sea ice variation. The atmospheric dynamic and thermodynamic contributions to extreme sea ice variation in different climate backgrounds need to be further investigated.

Acknowledgements The authors would like to thank National Snow and Ice Data Center, USA for providing the sea ice concentration data (https://nsidc.org/data), European Centre for Medium-Range Weather Forecasts for ERA5 monthly reanalysis data (https://cds.climate.copernicus.eu/cdsapp#!/search?type=dataset) and Key Laboratory of Polar Atmosphere-ocean-ice System for Weather and Climate, Ministry of Education, China. No conflict of interest exits in the submission of this manuscript. This work is supported by S&T Development Fund of CAMS (Grant no. 2023KJ018), Basic Research Fund of CAMS (Grant nos. 2023Z015 and 2023Z025), and Key Laboratory of Polar Atmosphere-ocean-ice System for Weather and Climate, Ministry of Education, China. We would like to thank two anonymous reviewers and Associate Editor Dr. Ruibo Lei for their helpful remarks.

References

Bhatt U S, Walker D A, Raynolds M K, et al. 2010. Circumpolar Arctic tundra vegetation change is linked to sea ice decline. Earth Interact, 14(8): 1-20, doi:10.1175/2010ei315.1.

Bi H B, Wang Y H, Liang Y, et al. 2021. Influences of summertime Arctic dipole atmospheric circulation on sea ice concentration variations in the Pacific sector of the Arctic during different Pacific decadal oscillation phases. J Clim, 34(8): 3003-3019, doi:10.1175/JCLI-D-19-0843.1.

Blackport R, Screen J A, van der Wiel K, et al. 2019. Minimal influence of reduced Arctic sea ice on coincident cold winters in mid-latitudes. Nat Clim Change, 9: 697-704, doi:10.1038/s41558-019-0551-4.

Cavalieri D J, Parkinson C L, DiGirolamo N, et al. 2012. Intersensor calibration between F13 SSMI and F17 SSMIS for global sea ice data records. IEEE Geosci Remote Sens Lett, 9(2): 233-236, doi:10.1109/LGRS.2011.2166754.

Chen D, Sun Q Z. 2024. Impact of rapid Arctic sea ice decline on China's crop yield under global warming. Environ Dev Sustain, 26(1): 1263-1280, doi:10.1007/s10668-022-02757-x.

Chen J L, Kang S C, Guo J M, et al. 2021. Variation of sea ice and perspectives of the Northwest Passage in the Arctic Ocean. Adv Clim Change Res, 12(4): 447-455, doi:10.1016/j.accre.2021.02.002.

Chen X D, Luo D H, Feldstein S B, et al. 2018. Impact of winter Ural blocking on Arctic sea ice: short-time variability. J Clim, 31(6): 2267-2282, doi:10.1175/jcli-d-17-0194.1.

Comiso J C, Parkinson C L, Gersten R, et al. 2008. Accelerated decline in the Arctic sea ice cover. Geophys Res Lett, 35(1): L01703, doi:10.1029/2007gl031972.

Comiso J C, Meier W N, Gersten R. 2017. Variability and trends in the Arctic sea ice cover: results from different techniques. J Geophys Res Oceans, 122(8): 6883-6900, doi:10.1002/2017jc012768.

Dai A, Luo D, Song M, et al. 2019. Arctic amplification is caused by sea-ice loss under increasing CO_2. Nat Commun, 10(1): 121, doi:10.1038/s41467-018-07954-9.

Dai A, Jenkins M T. 2023. Relationships among Arctic warming, sea-ice loss, stability, lapse rate feedback, and Arctic amplification. Clim Dyn, 61(11): 5217-5232, doi:10.1007/s00382-023-06848-x.

Francis J A, Wu B Y. 2020. Why has no new record-minimum Arctic sea-ice extent occurred since September 2012? Environ Res Lett, 15(11): 114034, doi:10.1088/1748-9326/abc047.

Gong T T, Luo D H. 2017. Ural blocking as an amplifier of the Arctic sea ice decline in winter. J Clim, 30(7): 2639-2654, doi:10.1175/jcli-d-16-0548.1.

Guarino M V, Sime L C, Schröeder D, et al. 2020. Sea-ice-free Arctic during the Last Interglacial supports fast future loss. Nat Clim Change, 10: 928-932, doi:10.1038/s41558-020-0865-2.

Holland M M, Bitz C M, Tremblay B. 2006. Future abrupt reductions in the summer Arctic sea ice. Geophys Res Lett, 33(23): L23503, doi:10.1029/2006gl028024.

Jenkins M T, Dai A G, Deser C. 2024. Seasonal variations and spatial patterns of Arctic cloud changes in association with sea ice loss during 1950–2019 in ERA5. J Clim, 37(2): 735-754, doi:10.1175/jcli-d-23-0117.1.

Jiang Z N, Feldstein S B, Lee S. 2021. Two atmospheric responses to winter sea ice decline over the Barents–Kara Seas. Geophys Res Lett, 48(7): e2020GL090288, doi:10.1029/2020gl090288.

Kendall M G. 1975. Rank correlation methods, 4th Edition. London: Charles Griffin.

Kwok R. 2018. Arctic sea ice thickness, volume, and multiyear ice coverage: losses and coupled variability (1958–2018). Environ Res Lett, 13(10): 105005, doi:10.1088/1748-9326/aae3ec.

Lee H J, Kwon M O, Yeh S W, et al. 2017. Impact of poleward moisture transport from the North Pacific on the acceleration of sea ice loss in the Arctic since 2002. J Clim, 30(17): 6757-6769, doi:10.1175/jcli-d-16-0461.1.

Liang X, Losch M. 2018. On the effects of increased vertical mixing on the Arctic Ocean and sea ice. J Geophys Res Oceans, 123(12): 9266-9282, doi:10.1029/2018jc014303.

Liu X H, Ma L, Wang J Y, et al. 2017. Navigable windows of the Northwest Passage. Polar Sci, 13: 91-99, doi:10.1016/j.polar.2017.02.001.

Luo B H, Luo D H, Wu L X, et al. 2017. Atmospheric circulation patterns which promote winter Arctic sea ice decline. Environ Res Lett, 12(5): 054017, doi:10.1088/1748-9326/aa69d0.

Luo B H, Luo D H, Ge Y, et al. 2023. Origins of Barents–Kara sea-ice interannual variability modulated by the Atlantic pathway of El Niño-Southern Oscillation. Nat Commun, 14(1): 585, doi:10.1038/s41467-023-36136-5.

Mann H B. 1945. Nonparametric tests against trend. Econometrica, 13(3): 245-259, doi:10.2307/1907187.

McGraw M C, Blanchard-Wrigglesworth E, Clancy R P, et al. 2022.

Understanding the forecast skill of rapid Arctic sea ice loss on subseasonal time scales. J Clim, 35(4): 1179-1196, doi:10.1175/jcli-d-21-0301.1.

Mohammadi-Aragh M, Goessling H F, Losch M, et al. 2018. Predictability of Arctic sea ice on weather time scales. Sci Rep, 8(1): 6514, doi:10.1038/s41598-018-24660-0.

Notz D, Stroeve J. 2016. Observed Arctic sea-ice loss directly follows anthropogenic CO_2 emission. Science, 354(6313): 747-750, doi:10.1126/science.aag2345.

Park D S R, Lee S, Feldstein S B. 2015. Attribution of the recent winter sea ice decline over the Atlantic sector of the Arctic Ocean. J Clim, 28(10): 4027-4033, doi:10.1175/JCLI-D-15-0042.1.

Park H S, Lee S, Son S W, et al. 2015. The impact of poleward moisture and sensible heat flux on Arctic winter sea ice variability. J Clim, 28(13): 5030-5040, doi:10.1175/jcli-d-15-0074.1.

Parkinson C L, Cavalieri D J. 2012. Antarctic sea ice variability and trends, 1979–2010. Cryosphere, 6(4): 871-880, doi:10.5194/tc-6-871-2012.

Post E, Bhatt U S, Bitz C M, et al. 2013. Ecological consequences of sea-ice decline. Science, 341(6145): 519-524, doi:10.1126/science.1235225.

Qian S M, Zhang L J, Yang B, et al. 2020. Analysis of intraseasonal oscillation characteristics of Arctic summer sea ice. Geophys Res Lett, 47(5): e2019GL086555, doi:10.1029/2019gl086555.

Serreze M C, Stroeve J. 2015. Arctic sea ice trends, variability and implications for seasonal ice forecasting. Philos Trans A Math Phys Eng Sci, 373(2045): 20140159, doi:10.1098/rsta.2014.0159.

Serreze M C, Holland M M, Stroeve J. 2007. Perspectives on the Arctic's shrinking sea-ice cover. Science, 315(5818): 1533-1536, doi:10.1126/science.1139426.

Simmonds I. 2015. Comparing and contrasting the behaviour of Arctic and Antarctic sea ice over the 35 year period 1979–2013. Ann Glaciol, 56(69): 18-28, doi:10.3189/2015aog69a909.

Spreen G, Kwok R, Menemenlis D. 2011. Trends in Arctic sea ice drift and role of wind forcing: 1992–2009. Geophys Res Lett, 38(19): L19501, doi:10.1029/2011gl048970.

Stroeve J, Holland M M, Meier W, et al. 2007. Arctic sea ice decline: faster than forecast. Geophys Res Lett, 34(9): L09501, doi:10.1029/2007gl029703.

Stroeve J, Serreze M, Drobot S, et al. 2008. Arctic sea ice extent plummets in 2007. EoS Transactions, 89(2): 13-14, doi:10.1029/2008eo020001.

Sumata H, de Steur L, Divine D V, et al. 2023. Regime shift in Arctic Ocean sea ice thickness. Nature, 615(7952): 443-449, doi:10.1038/s41586-022-05686-x.

Tian Y L, Zhang Y, Zhong D Y, et al. 2022. Atmospheric energy sources for winter sea ice variability over the North Barents–Kara Seas. J Clim, 35(16): 5379-5398, doi:10.1175/jcli-d-21-0652.1.

Tschudi M A, Stroeve J C, Stewart J S. 2016. Relating the age of Arctic sea ice to its thickness, as measured during NASA's ICESat and IceBridge campaigns. Remote Sens, 8(6): 457, doi:10.3390/rs8060457.

Tschudi M, Meier W N, Stewart J S, et al. 2019. Polar pathfinder daily 25 km EASE-Grid sea ice motion vectors (Version 4, Indicate subset used). Boulder: NASA National Snow and Ice Data Center Distributed Active Archive Center, doi: 10.5067/INAWUWO7QH7B.

Yang J, Li S Y, Zhu T, et al. 2022. Intraseasonal melting of northern Barents sea ice forced by circumpolar clockwise-propagating atmospheric waves during early summer. J Clim, 35(17): 5703-5718, doi:10.1175/JCLI-D-21-0538.1.

Yang W, Magnusdottir G. 2017. Springtime extreme moisture transport into the Arctic and its impact on sea ice concentration. J Geophys Res Atmos, 122(10): 5316-5329, doi:10.1002/2016jd026324.

You C, Tjernström M, Devasthale A, et al. 2022. The role of atmospheric blocking in regulating Arctic warming. Geophys Res Lett, 49(12): e2022GL097899, doi:10.1029/2022gl097899.

Wang S Y, Liu J P, Cheng X, et al. 2023. Separation of atmospheric circulation patterns governing regional variability of Arctic sea ice in summer. Adv Atmos Sci, 40(12): 2344-2361, doi:10.1007/s00376-022-2176-1.

Wang Z, Walsh J, Szymborski S, et al. 2020. Rapid Arctic sea ice loss on the synoptic time scale and related atmospheric circulation anomalies. J Clim, 33(5): 1597-1617, doi:10.1175/JCLI-D-19-0528.1.

Wu B Y, Li Z K. 2022. Possible impacts of anomalous Arctic sea ice melting on summer atmosphere. Int J Climatol, 42(3): 1818-1827, doi:10.1002/joc.7337.

Zhang F Y, Pang X P, Lei R B, et al. 2022. Arctic sea ice motion change and response to atmospheric forcing between 1979 and 2019. Int J Climatol, 42(3): 1854-1876, doi:10.1002/joc.7340.

Zhang R N, Zhang R H, Dai G K. 2022. Intraseasonal contributions of Arctic sea-ice loss and Pacific decadal oscillation to a century cold event during early 2020/21 winter. Clim Dyn, 58(3): 741-758, doi:10.1007/s00382-021-05931-5.

Zheng C, Ting M F, Wu Y T, et al. 2022. Turbulent heat flux, downward longwave radiation, and large-scale atmospheric circulation associated with wintertime Barents–Kara Sea extreme sea ice loss events. J Clim, 35(12): 3747-3765, doi:10.1175/jcli-d-21-0387.1.

Zhong L H, Hua L J, Luo D H. 2018. Local and external moisture sources for the Arctic warming over the Barents–Kara Seas. J Clim, 31(5): 1963-1982, doi:10.1175/JCLI-D-17-0203.1.